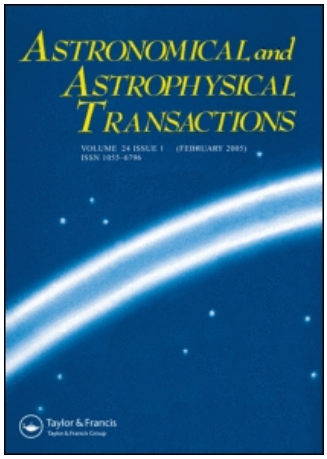

Astronomical & Astrophysical Transactions
The Journal of the Eurasian Astronomical Society
Publication details, including instructions for authors and subscription information:
http://www.informaworld.com/smpp/title~content=t713453505

A kinematical study of R aquarii jet features

G. Bodo [a]; L. Errico [b]; S. Massaglia [a]; P. Rossi [a]; E. Trussoni [a]; A. A. Vittone [b]
[a] Osservatorio Astronomico di Torino, Pino Torinese, TO, Italy
[b] Osservatorio Astronomico di Capodimonte, Napoli, Italy

Online Publication Date: 01 April 1998
To cite this Article: Bodo, G., Errico, L., Massaglia, S., Rossi, P., Trussoni, E. and Vittone, A. A. (1998) 'A kinematical study of R aquarii jet features', Astronomical & Astrophysical Transactions, 17:4, 321 - 331
To link to this article: DOI: 10.1080/10556799808232098
URL: http://dx.doi.org/10.1080/10556799808232098

Astronomical and Astrophysical Transactions, 1998, Vol. 17, pp. 321–331
Reprints available directly from the publisher
Photocopying permitted by license only

A KINEMATICAL STUDY OF R AQUARII JET FEATURES

G. BODO[1], L. ERRICO[2], S. MASSAGLIA[1], P. ROSSI[1], E. TRUSSONI[1], and A. A. VITTONE[2]

[1] *Osservatorio Astronomico di Torino, Strada dell'Osservatorio 20, I-10025 Pino Torinese (TO), Italy*

[2] *Osservatorio Astronomico di Capodimonte, Via Moiariello 16, I-80131 Napoli, Italy*

(Received November 11, 1997)

We performed high-resolution spectroscopic observations of R Aqr jets in 1989 and 1990. Radial velocity fields along the jet direction are obtained. These reveal a proper motion of $0''.5 \pm 0''.3$ per year of the emitting features located at a distance of about $10''$ from the centre of the inner nebula. We also discuss the possible mechanisms producing the observed proper motion and the problem of the origin of the supersonic jet.

KEY WORDS Symbiotic stars: R Aqr, jets

1 INTRODUCTION

R Aqr is a D-type symbiotic system (Kenyon, 1986; Michalitsianos, 1984) at a distance of about 250 pc (Lépine *et al.*, 1978; Whitelock, 1987). It consists of a bright oxygen-rich Mira whose light varies over a 387 day period and a hot stellar source at an intermediate phase between a subwarf and a white dwarf (Burgarella *et al.*, 1992).

R Aqr is at the centre of a slowly expanding nebula (Hubble, 1943; Baade, 1944) with an outer region extending $\sim 2'$ in the east–west direction and an inner region extending $\sim 1'$ in the north–south direction (Sopka *et al.*, 1982). Within the inner region a spike of emission resembling a jet oriented along the north–east direction appeared around 1977 (Wallerstein and Greenstein, 1980; Herbig, 1980). This feature was first studied in optical and radio regions by Sopka *et al.* (1982), who found it extends $\sim 10''$ from the nucleus and appears ~ 10 times as bright as the surrounding features of the nebula.

High-resolution maps of the jet showing considerable detail were obtained at 6 cm wavelength with the VLA (Kafatos *et al.*, 1983), in the near UV region (Mauron *et al.*, 1985) and in the optical region (Paresce *et al.*, 1988; Burgarella and

Paresce, 1991). The VLA observations showed that the jet consists of five components, while narrow-band Hα imaging revealed a sixth component. Spectra of the jet secured by Herbig (1980) showed a radial velocity of the knots of $\sim$ 70 km s^{-1} whereas spectra of the central object gave a lower velocity ($\sim$ 44 km s^{-1}). Kafatos *et al.* (1989) detected a collimated amorphous radio continuum structure, which extends $\sim$ 10″ S–W of R Aqr. The detection provides strong evidence for a symmetrical or bipolar jet phenomenon. An upper limit of $\sim$ 0.″3 per year was derived for the proper motion of the jet components (Mauron *et al.*, 1985). Strong variations in the brightness and kinematical properties of the jet components were observed (Solf, 1992). New VLA observations (Lehto and Johnson, 1992) showed that the positions of five of the six radio components had changed, revealing proper motions. The tangential velocity varies from 44 to 160 km s^{-1} with respect to the Mira. High-resolution images of the core of R Aqr were secured with the FOC on the Hubble Space Telescope (HST) (Paresce *et al.*, 1991; Paresce and Hack, 1994) detecting motions of about 200 km s^{-1}. Recently, MERLIN radio observations, comparable to the resolution of the HST images, have shown that the outflow velocity must be of at least 300 km s^{-1} (Dougherty *et al.*, 1995).

Several models were proposed to explain the appearance of the jet features in the R Aqr system. These models, according to the source of jet excitation, can be divided into shock and photoionization models. An up-to-date review of R Aqr models can be found in Burgarella *et al.* (1992).

In Section 2 we outline the long-slit spectroscopic observations secured with the aims of obtaining a radial velocity map of the jet region and of monitoring the time evolution of the jet features. The results are presented in Section 3. In Section 4 we discuss different pictures for the interaction of the jet with the nebular medium that may explain, at least partially, the observations presented in this paper. We present also a model for the origin of the jet in terms of magnetic acceleration and collimation by a rotating compact object.

2 OBSERVATIONS AND DATA REDUCTION

In order to obtain accurate radial velocities of the jet features around R Aqr we performed two high-resolution spectroscopic observational runs in October 1989 and October 1990. At these epochs the phases of the Mira light curve were 0.18 and 0.79 respectively. The observations were carried out using the echelle spectrograph attached to the 1.82 m telescope of Asiago Astrophysical Observatory, Italy.

In the first observational run the position angle (P.A.) of the 75″ long slit was set at 30° and centred on the star. The slit width was 200μ, i.e. $\sim$ 2.5″, and covered completely the blobs A and B, and partially the blob D (Figure 1). This slit position corresponds approximately at 8 and 9 positions shown in Figure 1 of Solf (1992). In the second run the slit was firstly put in the same position as the first run and then rotated around the star at different position angles by steps of 30°. The log of observations is shown in Table 1.

Table 1. Log of observations

Date	*P.A.* (°)	*Spectral range* (Å)	*Dispersion* (Å mm^{-1})	*Exp. time* (*sec*)
22 Oct 89	30	4813–4905	7.65	2700
22 Oct 89	30	4923–5016	7.78	2700
23 Oct 89	30	6516–6640	10.37	1800
9 Oct 90	30	6508–6632	10.37	1800
9 Oct 90	120	6508–6632	10.37	1800
9 Oct 90	60	6508–6632	10.37	1800
9 Oct 90	90	6508–6632	10.37	1800

The pixel size of the CCD detector was 23μ and the scale perpendicular to the dispersion was $27''$/mm, corresponding to $0.''6$/pixel on the sky. The spatial resolution of the spectra was seeing limited (about $2.''5$ at the epochs of our observations). Only in the region very close to the star did the strong emission of the Mira spread out on the CCD.

Selected spectral ranges were observed in order to secure some of the main characteristic emission lines of the optical spectrum of the R Aqr, namely Hα, [N II] 6548, 6584Å and [O III] 4959, 5007Å.

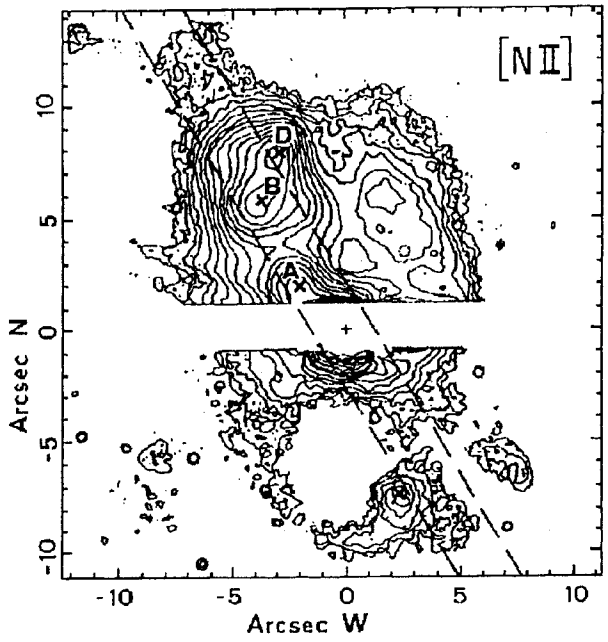

Figure 1 [N II] 6583 contour map of the inner R Aqr nebula (adapted from Figure 4 of Paresce *et al.*, 1988). The included area between the broken lines indicates the sky zone covered by the spectrograph slit set to P.A. = 30°.

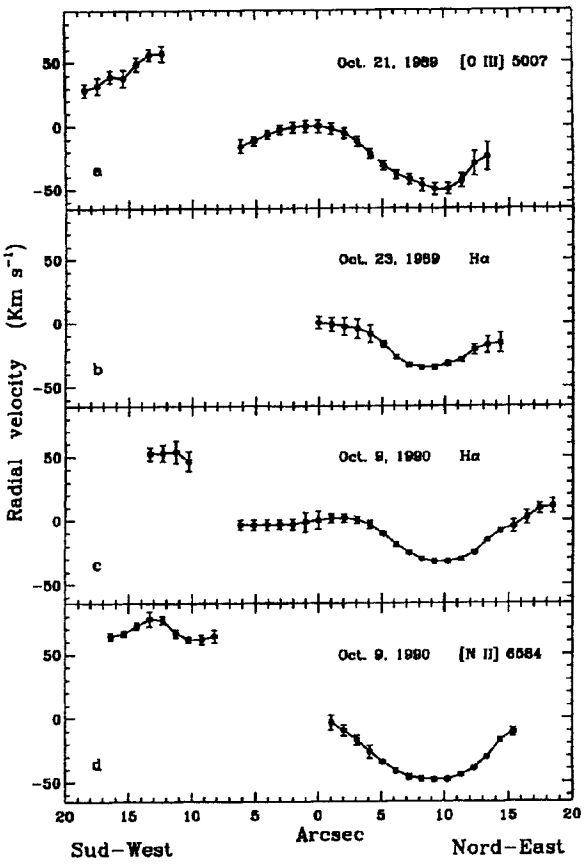

Figure 2 Radial velocities measured within the inner R Aqr nebula with spectrograph slit angle set to 30° N–E. Velocities are relative to the centre of the symbiotic system. The distance from the Mira star is on the abscissa. The error bars of each measurement are drawn.

An analysis of the spectra was performed in order to find the best radial velocity determinations at different distances from the star. Appropriate software was developed to correct the distortion due to the spectrograph. The Mira spectrum is clearly recognized from both the continuum emission and typical molecular absorption bands. The spread function due to seeing (about 4 pixels covered within 1σ a perpendicularly to the dispersion) is peaked enough so that we can reasonably determine the centre of the Mira position and superimpose the different spectra with an one-pixel spatial accuracy. A second-order polynomial is used to fit the shape of the Mira spectrum, so the echelle spectra are straightened and aligned in the columns of the image matrices. Then the wavelength calibration is independently made column by column so as to prevent errors due to the distortion along the direction perpendicular to the dispersion. The radial velocity and the equivalent width of emission lines are sampled with a step of about $1''$ starting from the star

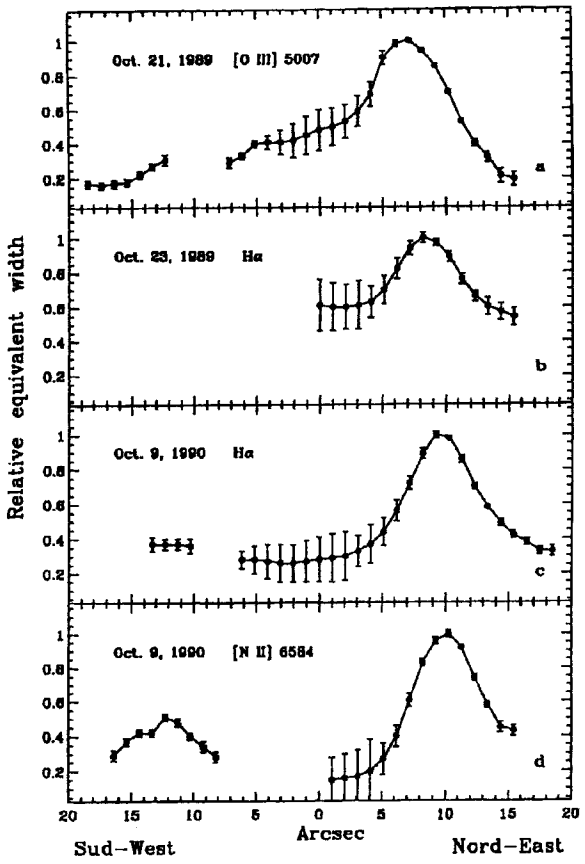

Figure 3 Equivalent widths measured within the inner R Aqr nebula with spectrograph slit angle set to 30° N–E. Equivalent widths are normalized to the maximum measured for each emission line. The distance from the Mira star is on the abscissa. The error bars of each measurement are drawn.

according to the limit due to seeing. The measures of radial velocity are referred to the line barycentre because all jet lines are not symmetrical due to different components along the sight line.

3 RESULTS

Figures 2 and 3 show the radial velocities and the equivalent widths of Hα, [N II] 6584Å and [O III] 5007Å emission lines, measured in the spectra recorded 30° from north towards the east, versus the distance from the Mira star. The region projected on the Mira centre is assumed as zero point for the velocities of the jet structures. Equivalent widths are given in relative intensities normalized to the

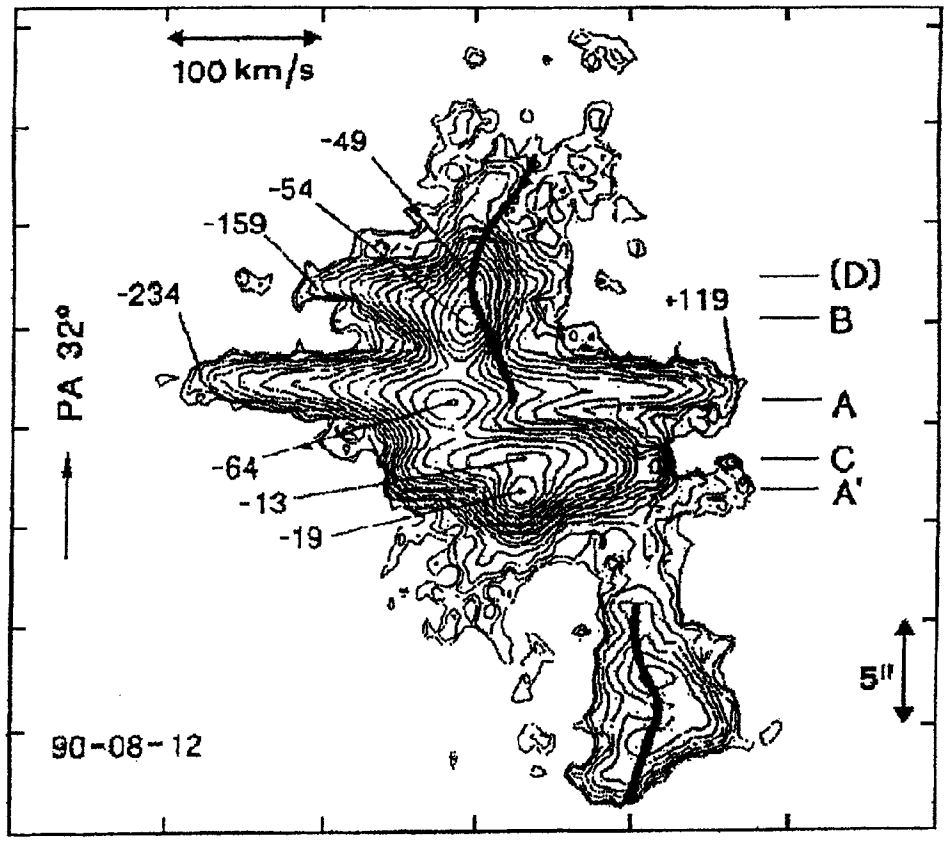

Figure 4 Comparison between the radial velocity of the [N II] 6583 line measured at P.A. = 30° in October 1990 (solid line superimposed on the contour levels) and the position–velocity diagram obtained at P.A. = 32° two months before by Solf (1992).

maximum emission of each line. That is because the continuum outside the star is always lower than the background, hence it is not possible to obtain equivalent widths in absolute values. The measure errors (shown in figures) are mainly due to signal/noise ratio of the emission lines.

In the spectra the emission lines disappear farther than 20″ from the star. The slit of the spectrograph was long enough to cover the whole jet feature on the sky. The possible optical emission from this feature inside the so-called outer nebula is not intense enough for our instrumental sensitivity. Anyway the emission from the feature at $\sim$ 7″ north–east of the star, already detected both in the optical range by Paresce *et al.* (1988) and in the radio range by Kafatos *et al.* (1983), is clearly recognized. Figure 4 shows our radial velocity profile of the [N II] line (Figure 2(*d*)) superimposed on the almost coeval map obtained by Solf (1992) for P.A. = 32°. Our results look mainly at the condensations B and D

of the jet-like feature. The light of the Mira and the seeing-limited spatial resolution prevent us obtaining believable results on the components A and A′ very close to the centre of the system. There is a very good agreement looking at the counter-jet feature present to the south–west of R Aqr. The distance from the central star and the radial velocity are comparable with those of the NE main jet feature at opposite position, but its emission is much lower. The origin of this jet is probably due to the same event responsible for the NE jet formation but the density of the SW jet region is lower as also suggested by Burgarella *et al.* (1992).

Comparing the jet velocity fields obtained from the Hα emission line at a distance of one year (Figure 2(b,c)), we find out that the shapes of these fields between $\sim 5''$ and $\sim 14''$ from the star are very similar but shifted by $0''.5 \pm 0''.3$. An analogous shift is shown (Figure 3) by the maximum of the Hα line equivalent width. At a distance of 250 pc this shift corresponds to a tangential velocity $v_t \approx 550 \pm 300$ km s^{-1}. We recall that Paresce and Hack (1994) derived from the proper motion of the A component ($4''$ from the Mira) a velocity of about 200 km s^{-1}.

A difference between the maximum radial velocities measured by the neutral hydrogen (~ 33 km s^{-1}) and by the forbidden lines [O III] and [N II] (~ 50 km s^{-1}) is present. This could mean that the shock front interacts in the jet region with a zone at different density and produces on each of these a different velocity. The different effects of the wave front on the excitation and acceleration of the matter around R Aqr are shown in Figure 2(a) and Figure 3(a). In the [O III] line the maximum of the radial velocity profile precedes the one of the equivalent width by more than $3''$.

No remarkable results have been obtained by the analysis of spectra recorded with the slit in other angle positions.

4 DISCUSSION

The proper motion detected at a distance $\sim 10''$ from the centre of the inner nebula is consistent with the composite structure of R Aqr: a collimated jet, originating from the compact companion of a Mira star, interacts with the ambient nebular medium leading to the formation of the blobs B and D. However, the present observation reveals a large difference between the velocities deduced from the Doppler shifts and from the proper motion. Furthermore the value of the tangential velocity (~ 550 km s^{-1}) is higher than those obtained in previous observations (see e.g. Solf, 1992).

In the following we will try to interpret these new features, focusing our attention on the supersonic jet-nebular gas interactions that could produce the observed proper motion. Thence we will discuss the possible origin of the jet itself.

4.1 The Jet's Interaction with the Ambient Medium

A supersonic jet can interact with the environment in several ways:

(1) the jet's head may strike into the nebular medium forming a bow shock that propagates forward, a second shock front propagates backward against the jet's flow and a contact discontinuity separates these two structures (Norman *et al.*, 1982);

(2) the jet can encounter on its journey dense clumps of nebular material, giving rise to a shock at the contact surface with the obstacle;

(3) the jet, if in pressure equilibrium with the surroundings, can develop Kelvin–Helmholtz instabilities that non linearly evolve into biconical shocks that travel along the jet (Bodo *et al.*, 1994); alternatively, temporal variations in the jet's speed may result in the formation of internal working surfaces leading to travelling shocks (Rees, 1978; Raga and Kofman, 1992).

Before going into more detail, we recall observational constraints that can be useful to identify, among the physical mechanisms listed above, the one that can reproduce the complex phenomenology that characterizes this object. A constraint comes from the shock strength: the excitation lines present in the spectrum are indicative of shock velocities in features B–D of $v_s < 500$ km s^{-1} (Solf, 1992). Secondly, the higher radial velocity observed for the [O III] lines (with higher excitation levels) with respect the Hα (Figures 2 and 3) may suggest that the structure of the bow shock must be with the apex in the forward direction, i.e., along the curved surface of shock the velocity and the shock strength have their maximum values at the apex, and decrease along the wings.

The speed with which the jet head drills its way into the external medium can be calculated by balancing the ram-pressure of the jet material at the head to that of the ambient matter (see, e.g., Norman *et al.*, 1982; Blondin *et al.*, 1989):

$$(v_j - v_h)^2 \rho_j \approx v_h^2 \rho_e \rightarrow v_h \approx \frac{\epsilon v_j}{1 + \sqrt{\nu}}, \tag{1}$$

where $\nu = \rho_e/\rho_j$ and $\epsilon \sim 1$ is a numerical parameter that takes into account the effects of the beam expansion at the head. The subscript j indicates the asymptotic values of velocity and density.

According to picture (1), a high-velocity jet ($v_j > v_t \approx 550$ km s^{-1}), forming an angle $\theta \leq 5°$ with respect to the plane of the sky, interacts with the inner nebula interiors. In fact, the low radial velocity observed ($\sim$ 40–50 km s^{-1}) implies that the jet is almost perpendicular to the line of sight. The shocked material, present at the head of the jet ("bow shock") and which is responsible of the observed emission lines, travels with a velocity $\geq v_h$ which, projected on to the plane of the sky, amounts to the observed proper motion of $0.5''$ in a year. Setting in equation (1) $\nu, \epsilon = 1$, one derives $v_j = 2v_h \approx 1100$ km s^{-1} (with $v_t \simeq v_h$). However the bow shock, while presenting the 'right' form with the apex in the forward direction, is

characterized by a speed consistent with lines with an excitation level higher than observed.

Picture (2) avoids this difficulty. In fact, one can envision a precessing jet with velocity $v_j = v_s \sim 500$ km s^{-1}, i.e. in agreement with the deduced shock velocity of Solf (1992), that terminates against the high density edge of the inner nebula giving rise to shocked emission. In this case the density of the nebular matter is much greater than the jet's, i.e. $\nu \gg 1$, therefore $v_h \ll v_j$, and the observed proper motion results from the shift of the projected terminal hot spot of the jet on the nebular edge as the jet precesses.

This second scheme would have the further advantage of linking the blue shift of the emission lines to the expansion velocity of the inner nebula edge; moreover it allows for shock velocities within the limit of the observations. However in this case the structure of the shock is opposite with respect to the previous one: the flow velocity now has its minimum value at the apex, which is directed toward the central body. Therefore the [O III] lines should have a lower velocity with respect to the Hα, in disagreement with the data.

In the above scenarios the radiation is supposed to originate at the head of the jet, but both cases disagree with observations. According to picture (3) instead jets can carry along internal shocks that take place either after non-linear evolution of Kelvin–Helmholtz instabilities (Bodo *et al.*, 1994) or following the formation of working surfaces due to variability in the central source (Rees, 1978; Raga and Kofman, 1992). These two mechanisms for the shock build up, even through quite different in the physical details, lead however to similar general pictures. In the case of "K–H" shocks, the jet's density and velocity determine the structure of the biconical shocks, i.e. the shock velocity, opening angle and proper motion. In the case of internal working surfaces, the shock velocity follows from the variability of the central source, while the shock plane at the jet's centre is perpendicular to the jet's longitudinal axis. In both cases the temperature distribution presents a maximum on the jet's axis, the origin of high excitation lines, and declines along wings that extend backwards at larger radii, leading to the "right" form of the emission, with the apex in the forward direction. In this last picture, the emitting feature we are observing is a jet's internal shock with a proper motion velocity $\approx v_t$, projected on the plane of the sky with an angle $\theta \leq 5°$, as in model (1); the jet velocity must be $v_j \geq v_t + v_s$, in order to reproduce the emission lines observed.

The observations by Paresce and Hack (1994) have shown that the morphology of the jet in the inner region of R Aqr (≤ 100 AU) is extremely complex. In particular, upstream of knot A a series of knots appears (N and S) with quite regular spatial distribution, negligible proper motions and variable brightness. From their spectral properties, these morphologies can be associated to internal shocks.

These observations may support the "internal shock" model. In fact, Kelvin–Helmholtz perturbations, with wavelengths of the order of the jet radius, can develop and grow on quite short timescales forming regularly spaced internal shocks. As shown in the numerical simulations by Bodo *et al.* (1994), these shocks eventually merge and, without disrupting the flow collimation, give rise to stronger shocks with longer separation scalelengths. Applying this physical behaviour to R Aqr,

one can therefore suggest that the innermost knots observed by HST results from short wavelength K–H, while the outermost A, B and D would be due to shock merging effects.

4.2 The Jet's Origin and Acceleration

The previous picture implies that the jet, originating from Mira's companion white dwarf, is collimated and with high velocity up to a distance of $\approx$ 2000 AU. Moreover the outflow appears already collimated at a distance $\leq$ 15 AU (Paresce and Hack, 1994). With respect to the origin and collimation processes discussed in Burgarella *et al.* (1992), we explore here an alternative mechanism based on the acceleration by a rotating, magnetized object, as proposed also for the origin of extragalactic and stellar jets. In fact, white dwarfs are rotating ($\Omega \geq 10^{-4}$ s^{-1}), magnetized objects ($B \leq 10^7$ gauss) such that the plasma can be effectively accelerated to high terminal velocities. The advantages of this process are:

(1) a very hot corona is not required (as in thermally driven winds) since the rotating magnetized body can create a flux of the Poynting vector;

(2) the rotation of the gas implies the presence of an azimuthal magnetic field that pinches the flow leading to its collimation very close to the central source.

We can deduce the general properties of a magnetized jet on the basis of the magnetohydrodynamic (MHD) description of steady asymmetric winds (Heyvaerts and Norman, 1989). If the jet is magnetically driven, its asymptotic velocity v_j is given by

$$v_j^2 \approx 2\Omega^2 r_A^2 \left(1 - \frac{v_A}{v_j}\right) - v_e^2 \tag{2}$$

where Ω is the angular velocity at the base of the streamline, v_e the escape speed, and v_A and r_A are the jet velocity and width at the transalfvenic point. For a white dwarf $v_e \approx 5 \times 10^8 (M_\odot/R_9)^{1/2}$ cm s^{-1}, where $M_\odot$ is the mass of the star in units of the solar mass, and R_9 its radius in units of 10^9 cm.

Since the observed proper motion implies a jet velocity $\ll v_e$, the two terms on the right hand side of equation (2) must be of the same order of magnitude. This allows us to obtain, from magnetic flux conservation, the following lower limit on the mass loss rate (taking into account that $v_j > v_A$):

$$\dot{m} = \pi \rho r^2 v > 2 \times 10^{-10} \frac{B_6^2 R_9^5 \Omega_{-3}^2}{M_\odot v_{j,8}} M_\odot/\mathrm{yr}, \tag{3}$$

where the velocity is expressed in units of 10^8 cm s^{-1}, the angular velocity in units of 10^{-3} s^{-1} and the magnetic field at the star surface in units of 10^6 G.

The above limit (3) is consistent with values derived from observations or independent theoretical arguments. From IUE observations, Michalitsianos *et al.* (1988) derived that a hot wind with velocity 700–1000 km s^{-1} and a mass loss rate 5×10^{-12}–$10^{-11} M_\odot$/yr may be present in R Aqr; while Henney and Dyson (1992) have estimated a mass loss rate $\sim 3 \times 10^{-10} M_\odot$/yr.

5 CONCLUSIONS

Our spectroscopic observations reveal radial velocities ≈ 50 km s^{-1} and a proper motion of $0.''5 \pm 0.''3$ (equivalent to a tangential velocity $\approx 550 \pm 300$ km s^{-1}), at a distance $\approx 10''$ from the centre, corresponding to the positions of blobs B and D. The radial velocity deduced from the neutral hydrogen line is lower by a factor ≈ 1.5 with respect the value obtained by the [N II] line.

The moving structure is likely to be a shock related to a jet moving at several hundred km s^{-1}, and lying almost perpendicular to the line of sight. We suggest that this shock is due to either K–H instabilities or an internal working surface connected with the variability of the outflow velocity.

The high-velocity jet can be effectively magnetically driven and collimated by the rotation of magnetized white dwarf orbiting the Mira star.

References

Baade, W. (1944) *Ann. Rep. Dir. Mt. Wilson Obs. 1943–1944*, 12.
Blondin, J. M., Königl, A., and Fryxell, B. A. (1989) *Astrophys. J.* **337**, 37.
Bodo, G., Massaglia, S., Ferrari, A., and Trussoni, E. (1994) *Astron. Astrophys.* **283**, 655.
Burgarella, D. and Paresce F. (1991) *Astrophys. J.* **370**, 590.
Burgarella, D., Vogel, M., and Paresce, F. (1992) *Astron. Astrophys.* **262**, 83.
Dougherty, S. M., Bode, M. F., Lloyd, H. M., Davis, R. J., and Eyres, S. P. (1995) *Mon. Not. Roy. Astron. Soc.* **272**, 843.
Henney, W. J. and Dyson, J. E. (1992) *Astron. Astrophys.* **261**, 301.
Herbig, G. (1980) *IAU Circ.* 3535.
Heyvaerts, J. and Norman, C. (1989) *Astrophys. J.* **347**, 1055.
Hubble, E. P. (1943) *Ann. Rep. Dir. Mt. Wilson Obs. 1942–1943*, 17.
Kafatos, M., Hollis, J. M., and Michalitsianos, A. G. (1983) *Astrophys. J.* **267**, L103.
Kafatos, M., Hollis, J. M., Yusef-Zadeh, F., Michalitsianos, A. G., and Elitzur, M. (1989) *Astrophys. J.* **346**, 991.
Kenyon, S. (1986) *The Symbiotic Stars*, Cambridge Univ. Press, Cambridge.
Lehto, H. J. and Johnson, D. R. H. (1992) *Nature* **355**, 705.
Lépine, J. R. D., Le Squeren, A. M., and Scalise, E. (1978) *Astrophys. J.* **225**, 869.
Mauron, N., Nieto, J. L., Picat, J. P., Lelievre, G., and Sol, H. (1985) *Astron. Astrophys.* **142**, L13.
Michalitsianos, A. G. (1984) *Comm. Astrophys.* **10**, 85.
Michalitsianos, A. G., Oliversen, R. J., Hollis, J. M., Kafatos, M., Crull, H. E., and Miller, R. J. (1988) *Astron. J.* **95**, 1488.
Norman, M. L., Winkler, K. A., Smarr, L., and Smith, M. D. (1982) *Astron. Astrophys.* **113**, 285.
Paresce, F. and Hack, W. (1994) *Astron. Astrophys.* **287**, 154.
Paresce, F., Burrows, C., and Horne, K. (1988) *Astrophys. J.* **329**, 318.
Paresce, F. *et al.* (1991) *Astrophys. J.* **369**, L67.
Raga, A. C. and Kofman, L. (1992) *Astrophys. J.* **386**, 222.
Rees, M. J. (1978) *Mon. Not. Roy. Astron. Soc.* **184**, 61.
Solf, J. (1992) *Astron. Astrophys.* **257**, 228.
Sopka, R. J., Herbig, G., Kafatos, M., and Michalitsianos, A. G. (1982) *Astrophys. J.* **258**, L35.
Wallerstein, G. and Greenstein, J. L. (1980) *Publ. Astron. Soc. Pac.* **92**, 275.
Whitelock, P. A. (1987) *Publ. Astron. Soc. Pac.* **99**, 573.